Journal of Statistical Physics, Vol. 77, Nos. 1/2, 1994

Surface-Directed Spinodal Decomposition in a Thin-Film Geometry: A Computer Simulation

Sanjay Puri[1,2] and Kurt Binder[2]

Received December 1, 1993; final March 24, 1994

The phase separation kinetics of a two-dimensional binary mixture at critical composition confined between (one-dimensional) straight walls which preferentially attract one component of the mixture is studied for a wide range of distances D between the walls. Following earlier related work on semiinfinite systems, two choices of surface forces at the walls are considered, one corresponding to an incompletely wet state of the walls, the other to a completely wet state (for $D \to \infty$). The nonlinear Cahn–Hilliard-type equation, supplemented with appropriate boundary conditions which account for the presence of surfaces, is replaced by a discrete equivalent and integrated numerically. Starting from a random initial distribution of the two species (say, A and B), an oscillatory concentration profile rapidly forms across the film. This is characterized by two thin enrichment layers of the preferred component at the walls, followed by adjacent depletion layers. While in these layers phase separation is essentially complete, the further oscillations of the average composition at distance Z from a wall get rapidly damped as Z increases toward the center of the film. This structure is relatively stable for an intermediate time scale, while the inhomogeneous structure in the center of the film coarsens. The concentration correlation function in directions parallel to the walls (integrated over all Z) and the associated structure factor (describing small-angle scattering from the film) exhibit a scaling behavior, similar to bulk spinodal decomposition, and the characteristic length scale grows with time as $l_{\|}(t) = \alpha + \beta t^a$, where a is close to the Lifshitz–Slyozov value 1/3, and the coefficients α, β depend on film thickness only weakly. Only when one considers the local correlation function at distances close to the walls are deviations from scaling observed due to the competing effects of the growing surface enrichment layers. However, at very late times [when $l_{\|}(t)$ becomes comparable to D] this bulklike description breaks down, and a concentration distribution is expected to be established which is a superposition of domains

[1] School of Physical Sciences, Jawaharlal Nehru University, New Delhi 110067, India (Permanent address).

[2] Institut für Physik, Johannes Gutenberg-Universität Mainz, D-55099 Mainz, Germany.

0022-4715/94/1000-0145$07.00/0

separated by interfaces perpendicular to the walls, the one type of domain being rich in A and nearly homogeneous, and the other poor in A except for two thin enrichment layers at the walls.

KEY WORDS: Spinodal decomposition; surface enrichment; wetting; coarsening; binary mixtures.

1. INTRODUCTION

While the kinetics of phase separation of bulk binary mixtures has found long-standing attention[1-13] (see refs. 1–4 for reviews), the effects of free surfaces or confining walls have been studied[14-26] only recently. As is well known, the preferential attraction of one species of a binary mixture by a wall may lead to wetting phenomena (see refs. 27–30 for reviews). Thus for a binary mixture that is confined between walls and undergoes phase separation there is a complicated interplay of the coarsening domains in the bulk of the film with growing wetting layers at the walls.[20,26,31] Furthermore, finite-size effects (when the characteristic linear dimension of the growing domains becomes comparable to the distance between the walls; see refs. 32 and 34–36 for general reviews) may also come into play at late times. Experiments[15-19,22,24] are even more difficult to interpret: first, in experimental systems the two surfaces of the film are usually not equivalent (e.g., one surface of the thin film is an interface with air or vacuum, the other with a solid substrate). Second, experimental systems involve rather complicated materials such as polymer mixtures, where surfaces may lead to additional complications (e.g., the polymers when adsorbed at the walls may change their conformation and exhibit a very different dynamic behavior.[29,37,38]) Third, attractive walls change the coexistence curve relative to the bulk phases (e.g., "capillary condensation"[39-41]) in a manner that is not explicitly known for these systems. Finally, given that the late stages of spinodal decomposition in bulk fluid mixtures are governed by hydrodynamic mechanisms,[1-3,42-44] one has to worry to what extent these mechanisms are operative in thin films.

Thus we feel there is a need to first clarify surface effects on spinodal decomposition in a thin-film geometry for simplified models, where the experimental complications listed above are absent. In this spirit, we consider a symmetrical binary solid mixture [microscopically it would be modeled by the Kawasaki[45] spin exchange kinetic Ising (SEKI) model, which has played a pivotal role already in promoting our understanding of spinodal decomposition in the bulk[1,7-10,13]] and choose two equivalent walls which exert on the mixture only a short-range surface force. Experimentally, one probably deals with long-range surface forces,[27,28]

but this is also a complication that we wish to avoid here. For this problem using a master equation approach[46] in a local mean-field approximation has led to the derivation of dynamical boundary conditions[14,20] which supplement the nonlinear Cahn–Hilliard[1,3,5] partial differential equation that describes spinodal decomposition in the bulk, and are hence consistent with the SEKI model but can also be justified in the critical region on much more general grounds.[21] We have used these boundary conditions in our study of surface effects in a semiinfinite geometry[26] and also use them here. We note that in some recent studies other boundary conditions are used *ad hoc* (e.g., ref. 47), but we do not consider this as a valid approach to the present problem, for reasons we have discussed elsewhere.[20]

This paper is organized in the following fashion. In Section 2 we define our model and introduce the quantities that we calculate in our computer simulations. As is well known, computer simulations have played a very important part in the development of the theory of bulk spinodal decomposition,[8–13] and this is the method of choice for the present problem also. Section 3 gives a detailed exposition of our numerical results. Section 4 ends this paper with a discussion and outlook for further work.

2. MODEL AND SIMULATION TECHNIQUE

As discussed in detail in refs. 14, 20, and 26, near the critical point of a binary mixture between two equivalent parallel walls at $Z=0$ and $Z=D$ one can describe the dynamics of the coarse-grained and rescaled concentration field $\Phi(\mathbf{R}, Z, \tau)$ by the dimensionless Cahn–Hilliard equation and dynamical boundary conditions as follows:

$$\frac{\partial \Phi(\mathbf{R}, Z, \tau)}{\partial \tau} = -\nabla^2 \left\{ \Phi(\mathbf{R}, Z, \tau) - [\Phi(\mathbf{R}, Z, \tau)]^3 + \frac{1}{2} \nabla^2 \Phi(\mathbf{R}, Z, \tau) \right\} \quad (1)$$

$$\begin{aligned} \frac{\partial \Phi(\mathbf{R}, Z=0, \tau)}{\partial \tau} = h_1 + g\Phi(\mathbf{R}, Z=0, \tau) + \gamma \left. \frac{\partial \Phi(\mathbf{R}, Z, \tau)}{\partial Z} \right|_{Z=0} \\ - \left(\frac{\gamma}{4}\right)^{2/3} \left. \frac{\partial^2}{\partial Z^2} \Phi(\mathbf{R}, Z, \tau) \right|_{Z=0} \\ - \frac{5}{6} \left(\frac{\gamma}{4}\right)^{1/3} \left. \frac{\partial^3 \Phi(\mathbf{R}, Z, \tau)}{\partial Z^3} \right|_{Z=0} = 0 \end{aligned} \quad (2)$$

$$\frac{\partial}{\partial Z} \left\{ \Phi(\mathbf{R}, Z, \tau) - [\Phi(\mathbf{R}, Z, \tau)]^3 + \frac{1}{2} \nabla^2 [\Phi(\mathbf{R}, Z, \tau)] \right\}_{Z=0} = 0 \quad (3)$$

$$\frac{\partial \Phi(\mathbf{R}, Z=D, \tau)}{\partial \tau} = h_1 + g\Phi(\mathbf{R}, Z=D, \tau) - \gamma \frac{\partial \Phi(\mathbf{R}, Z, \tau)}{\partial Z}\bigg|_{Z=D} - \left(\frac{\gamma}{4}\right)^{2/3} \frac{\partial^2}{\partial Z^2} \Phi(\mathbf{R}, Z, \tau)\bigg|_{Z=D} + \frac{5}{6}\left(\frac{\gamma}{4}\right)^{1/3} \frac{\partial^3 \Phi(\mathbf{R}, Z, \tau)}{\partial Z^3}\bigg|_{Z=D} = 0 \tag{4}$$

and

$$\frac{\partial}{\partial Z}\left\{\Phi(\mathbf{R}, Z, \tau) - [\Phi(\mathbf{R}, Z, \tau)]^3 + \frac{1}{2}\nabla^2[\Phi(\mathbf{R}, Z, \tau)]\right\}_{Z=D} = 0 \tag{5}$$

In these equations, $\mathbf{R}$ and Z are distances parallel and perpendicular to the wall, respectively, measured in units of twice the bulk correlation length ξ_b and are hence dimensionless. While the gradient operators for the nonlinear Cahn–Hilliard equation for the bulk order parameter [Eq. (1)] do not single out any direction in space, the boundary conditions (2)–(4) clearly make these coordinates $\mathbf{R}$, Z nonequivalent. Similarly, the order parameter field Φ is also dimensionless and rescaled by the saturation value of the order parameter at the coexistence curve. Finally, τ is a rescaled dimensionless time.[26] Obviously, by this rescaling any material-dependent parameters describing the bulk properties of the mixture have been absorbed into the scale factors relating Z, Φ, and τ to the corresponding microscopic parameters.[26]

It is obvious from this discussion that our film thickness D is not measured in angstroms (Å) but in units of $2\xi_b$ and hence is a dimensionless parameter. Thus the choice $D \gg 1$ is mandatory, because only then can we have well-separated domains, as the intrinsic domain wall thickness in mean-field theory is also given by $2\xi_b$.[49]

Since Eq. (1) is a fourth-order differential equation, it is natural that for the finite interval $\{0 \leqslant Z \leqslant D\}$ there are four boundary conditions, two at each boundary: this suffices to yield unique well-defined solutions to the initial value problem, where $\Phi(\mathbf{R}, Z, \tau = 0)$ is specified. This is the initial value problem we wish to solve, considering quenching experiments from a temperature far above the bulk critical temperature T_c (where the initial equilibrium state is homogeneous, apart from random statistical fluctuations) to a temperature T where the homogeneous state is thermodynamically unstable.

The boundary conditions (3) and (5) do not involve any parameters either and are trivially interpreted as a consequence of the conservation laws for the particle numbers for both species, implying that there cannot

be any concentration flux normal to the walls at $Z=0$ and $Z=D$: no particles are allowed to leave the confining thin-film geometry. The boundary conditions (2) and (4), however, do involve three parameters, h_1, g, and γ: in an Ising model language h_1 is a rescaled boundary magnetic field acting on the spins in the surface layers of the systems only.[50,51] In ref. 26 we have described in detail how in the framework of a lattice model for binary alloys this term arises as a consequence of missing neighbors near the wall (if pairwise interactions φ_{AA}, φ_{BB} between like AA, BB neighbors differ) and of the energy difference between the potential energies of A atoms and B atoms adjacent to the walls. While the quantity γ is again related to the bulk correlation length, $\gamma = 4\xi_b^3$, the quantity g also results from "missing neighbors" and in addition depends on the ratio J_s/J, where J_s denotes the strength of pairwise (nearest-neighbor) interactions in the planes adjacent to the walls, while J denotes the analogous quantity in the bulk of the thin film. Obviously, we have once more assumed that the wall changes the energetics of the model right in the layers adjacent to the walls only. However, our treatment could be extended to the case with long-ranged interactions relatively easily.

For $T \to T_c$, where this continuum description is reasonable since then ξ_b is much larger than the lattice spacing and only then higher-order terms neglected in Eqs. (1)–(5) are small,[14] it is obvious that in the static limit the boundary conditions reduce to

$$\left.\frac{\partial \Phi_s(\mathbf{R}, Z)}{\partial Z}\right|_{Z=0} = -\frac{h_1}{\gamma} - \frac{g}{\gamma}\Phi_s(\mathbf{R}, Z=0) \tag{6}$$

$$\left.\frac{\partial \Phi_s(\mathbf{R}, Z)}{\partial Z}\right|_{Z=D} = \frac{h_1}{\gamma} + \frac{g}{\gamma}\Phi_s(\mathbf{R}, Z=D) \tag{7}$$

where we have neglected higher-order gradients. In the bulk, the static order parameter $\Phi_s(\mathbf{R}, Z)$ satisfies the equation[49,50,26]

$$\Phi_s(\mathbf{R}, Z) - [\Phi_s(\mathbf{R}, Z)]^3 + \tfrac{1}{2}\nabla^2 \Phi_s(\mathbf{R}, Z) = \text{const} \tag{8}$$

The resulting phase diagram of this model has been discussed extensively in the literature. For $D \to \infty$, one finds in the plane of variables h_1/γ, g/γ a dividing line, namely the line of wetting phase transitions, separating the regime where the walls are incompletely wet (or dry, respectively) from the regime where they are wet (dry).[27–29,49,50] For $g/\gamma < -2$ one has second-order wetting, while for $g/\gamma > -2$ one has first-order wetting. For $g/\gamma > -2$ one also finds prewetting at compositions slightly off-coexistence in the one-phase region.

For finite D, the phase coexistence between the A-rich and B-rich

phases occurs at compositions different from the bulk[38–40] and the critical wetting transition is rounded. Only the prewetting transition may still be present[51] for large enough D.

In order to characterize the dynamical behavior of the phase-separating system after the quench, it is convenient to introduce the following correlation functions[26] (we specialize to the case of a two-dimensional system here, where $\mathbf{R}$ has only one component X)

$$G_{||}(X_1 - X, Z, \tau) = \langle \Phi(X_1, Z, \tau)\, \Phi(X, Z, \tau) \rangle - \langle \Phi \rangle^2 \tag{9}$$

Note that although we consider an equal-time correlation function, there is a time dependence since we treat a nonequilibrium relaxation process following a sudden quench. A characteristic length scale parallel to the walls $l_{||}(Z, \tau)$ can be obtained from the correlation function as follows:[26]

$$G_{||}(l_{||}(Z, \tau), Z, \tau) = G_{||}(0, Z, \tau)/2 \tag{10}$$

Another quantity of interest is the integrated correlation function, which is the average of Eq. (9) over all values of Z,

$$G^{\text{int}}(X_1 - X, \tau) = \int_0^D G_{||}(X_1 - X, Z, \tau)\, dZ/D \tag{11}$$

Again we may define an associated length scale $l^{\text{int}}(\tau)$ by

$$G^{\text{int}}(l^{\text{int}}(\tau), \tau) = G^{\text{int}}(0, \tau)/2 \tag{12}$$

Note that in Eqs. (9)–(12) we have explicitly made use of the translational invariance of the system in the direction parallel to the walls (realized in the numerical simulation by periodic boundary conditions). Thus it also makes sense to consider a Fourier transform, describing the intensity of small-angle scattering with a scattering vector $\mathbf{k}$ oriented parallel to the walls,

$$S^{\text{int}}(k_x, \tau) = \int_{-\infty}^{+\infty} dX \exp(iXk_x)\, G^{\text{int}}(X, \tau) \tag{13}$$

These will be the quantities studied in the following section, in addition to the laterally averaged order parameter profile, $\Phi_{\text{av}}(Z, \tau)$, defined as

$$\Phi_{\text{av}}(Z, \tau) = \int_0^{L_x} \Phi(X, Z, \tau)\, dX/L_x \tag{14}$$

L_x is the linear dimension of the simulated system in the X direction (we use $L_x = 600$ throughout). Additional quantities have been defined[26] and evaluated, but we do not present these here.

We now make a few general remarks regarding the numerical methods we use to solve Eqs. (1)–(5). We have implemented an Euler-discretized version of these equations with an isotropically discretized Laplacian on two-dimensional lattices of size $L_x \times D$ where $L_x = 600$.[11,26] Similarly the boundary conditions (2) and (3) are implemented at $Z = 0$ and Eqs. (4) and (5) at $Z = D$, with D ranging from 30 to 90. The mesh sizes of our discretization are $\Delta\tau = 0.05$ and $\Delta X = \Delta Z = 1.5$. Of course, these mesh sizes are too coarse to simulate accurately the original partial differential equation. Thus, this discrete model should be understood in the spirit of cell-dynamical system (CDS) models, which provide a discrete space-time description that is dynamically equivalent to the continuum description.[11]

The mesh sizes are also too coarse to reproduce the precise short-wavelength structure near the walls.[26] However, as already demonstrated in previous work, the time scales of growth of the enrichment (and depletion) layers adjacent to the surfaces are much slower than the time scale of phase separation for our choice of parameters and when the surface forces are short ranged. As in ref. 26, we choose $\gamma = 4$, $g = 4$, and two choices of h_1 namely $h_1 = 4$ (this corresponds to an incompletely wet equilibrium of a surface in a semiinfinite system) and $h_1 = 8$ (this corresponds to a choice of an equilibrium state deep in the wet phase for a semiinfinite system).

We have also carried out a simulation with a distinctly finer mesh, namely $\Delta Z = 0.6$ and $\Delta\tau = 0.001$, but only for the one-dimensional case. In this case the simulation can be run up to "equilibrium," which is reached at times of the order of $\tau \approx 10^4$. However, already at this point we make the caveat that such a one-dimensional simulation can describe only those equilibrium states which are homogeneous in the X direction. This is not expected to be the case for our model, as will be discussed in some detail in Section 4.

We finally emphasize that for the time range studied ($\tau \leqslant 4000$) any finite-size effects associated with our choice of $L_x = 600$ can be safely ignored. This fact has been checked explicitly in our previous study of semi-infinite systems,[26] where also sizes $L_x = 150$ and $L_x = 300$ were used. All results for profiles, correlation functions, and structure factors are averages over 200 independent initial conditions. Each initial condition consists of uniformly distributed random fluctuations of $\Phi(X, Z, \tau = 0)$ of amplitude ± 0.025 about a zero background. Our simulation thus simulates a "critical quench" (the average value of Φ stays zero throughout, i.e., the mixture is at the critical composition of our system for $D \to \infty$), with an initial condition at "infinite temperature" (or in a state in the one-phase region with a correlation length ξ_b distinctly smaller than at the temperature to which the system is quenched).

3. NUMERICAL RESULTS

We begin by presenting our numerical data for the case $h_1 = 4$ (corresponding to an incompletely wet static equilibrium). Figure 1 illustrates the time evolution of our discrete model by presenting snapshot pictures for two thicknesses. One sees, even for very early times, the systems have formed enrichment layers at the walls which are approximately two cells wide, i.e., of thickness $2\Delta Z = 3$ (remember that lengths are measured in units of $2\xi_b$). These layers hardly change during the displayed time evolution at all [only when one studied the profiles of $\Phi_{av}(Z, \tau)$ with a much finer mesh size can one see a slow growth of the thickness of these surface enrichment layers with time[26]]. These enrichment layers are followed by adjacent depletion layers of the same thickness: the material adsorbed at the surface in these enrichment layers is simply transported from the closest possible distances to the walls. Qualitatively the same behavior has been found analytically and numerically for the kinetics of surface enrichment in the one-phase region.[14,20] These depletion layers are followed by another enrichment layer further inside the films. Initially, these second enrichment layers have about the same thickness as the layers directly adjacent to the walls, and have minor irregularities in the X direction parallel to the walls only. However, later, the thickness of this structure grows, as do the linear dimensions of the domains in the center of the thin film. Furthermore, during the coarsening process, domains of negative order parameter formed in the bulk of the film coalesce with the depletion layer mentioned above. At the later stages for the thinner film ($D = 30$) we can already recognize situations where locally there are only A-rich zones at the walls, while the A-poor region extends throughout the film in the perpendicular direction, connecting the right and the left depletion zones in the thin film with each other. If one could run the simulation long enough, we expect that the film would ultimately decompose into a succession of A-rich domains (which would be plug-shaped and uniformly black in the snapshot picture) separated by A-poor domains of about the same size (which are also plug-shaped and uniformly white in the center, but "decorated" with surface enrichment layers rich in A—i.e., black regions in the snapshot—at the domain walls).

These observations from single snapshots are made more quantitative when one considers the time evolution of the laterally averaged order parameter profiles $\Phi_{av}(Z, \tau)$, which are shown in Fig. 2 (recall that these data are based upon 200 independent time evolutions of the type shown in Fig. 1). The approximate time independence of the enrichment layers adjacent to the walls followed by similar nearly time-independent depletion zones is clearly seen. The boundary conditions at the surface thus have a

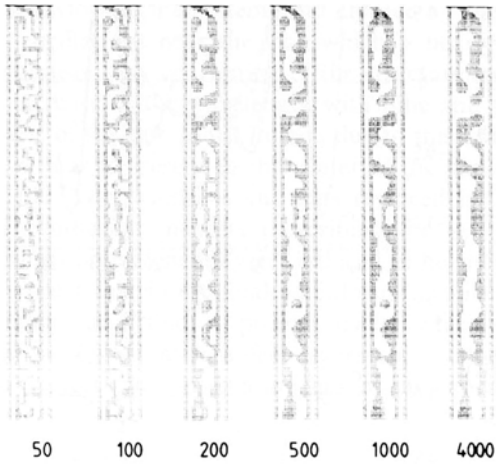

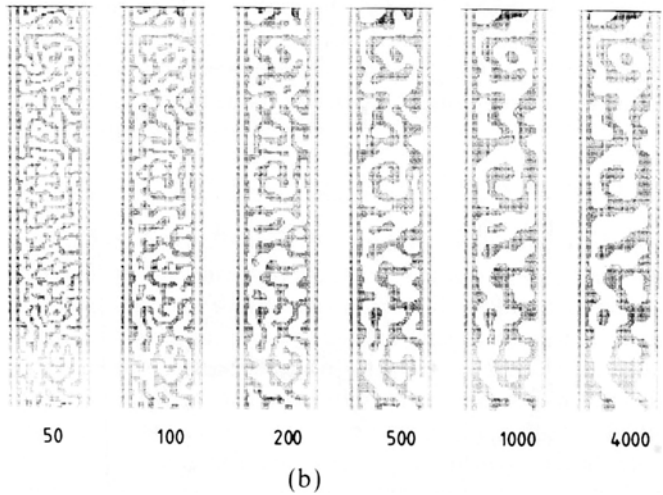

Fig. 1. Pictures of the time evolution from one discrete Euler implementation (with $\Delta X = 1.5$, $\Delta\tau = 0.05$) of the partial differential equation [Eqs. (1)–(5)] on the square lattice in a $D \times L_x$ geometry, with $L_x = 600$ and $D = 30$ (a) and $D = 60$ (b). The snapshots refer to the scaled times (from left to right) $\tau = 50$, 100, 200, 500, 1000, and 4000. Positive values of the order parameter are shown in black, while negative values are not marked. The parameter values chosen are $\gamma = 4$, $g = -4$, and $h_1 = 4$, which correspond to an incompletely wet static equilibrium in a semiinfinite geometry.

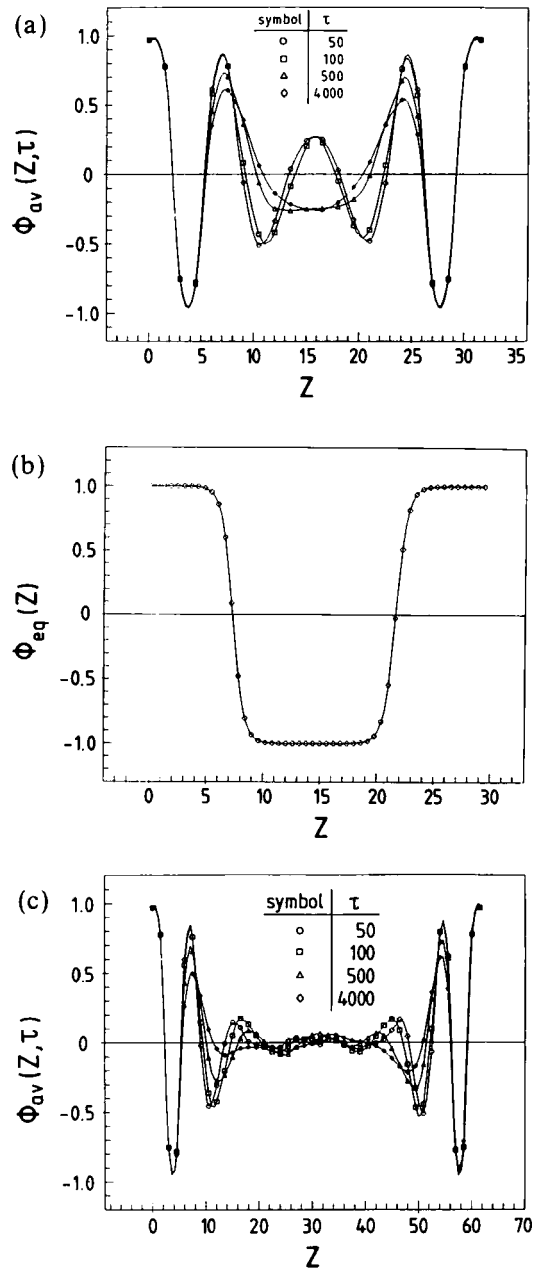

Fig. 2. Averaged order parameter profiles $\Phi_{av}(Z, \tau)$ plotted vs. the dimensionless distance Z from the first wall for four different scaled times as indicated, for $D = 30$ (a) and $D = 60$ (c). Data are obtained as an average over 2000 independent initial conditions. (b) The final stage of a one-dimensional calculation with a fine grid ($\Delta Z = 0.6$, $\Delta t = 0.001$) for $D = 30$ is shown for purposes of comparison. Parameters chosen are $\gamma = 4$, $g = -4$, and $h_1 = 4$, i.e., the same values as in Fig. 1.

very dominant behavior on the system, and enforce a "wavelength" of the order parameter oscillations near the wall which is nearly independent of time and film thickness. Any coarsening of the structure in the Z direction would mean an increase of the wavelength with time and this is seen only in the interior parts of the thin films. In fact, due to this coarsening, a maximum of $\Phi_{av}(Z, \tau)$ that is present in the center of the film with $D = 30$ for early times ($\tau \leqslant 100$) later vanishes and gets replaced by a minimum for times $\tau \geqslant 400$. The adjacent maxima (describing the two interior enrichment layers described above) steadily get reduced in height for both $D = 30$ and $D = 60$. We expect that in the final equilibrium profile these structures disappear altogether, and that a profile results which decreases from $\Phi_{eq}(Z = 0) = \Phi_{eq}(Z = D) \approx 1$ after a few layers to a value slightly below zero, in order to respect the conservation law of the concentration, which requires

$$\int_0^D \Phi_{av}(Z, \tau)\, dZ = \int_0^D \Phi_{eq}(Z)\, dZ = 0 \tag{15}$$

As discussed above, this (hypothetical) equilibrium profile results from a superposition of A-rich domains, which basically have $\Phi_{eq}^{+}(Z) \approx 1$ for all Z, and A-poor domains, which have $\Phi_{eq}^{-}(Z) \approx 1$ for $0 < Z \lesssim 3$, $D - 3 < Z \lesssim D$ (the enrichment layers), and $\Phi_{eq}^{-}(Z) \approx -1$ elsewhere: The volume fractions P_+, P_- of these two types of domains are then adjusted such that the laterally averaged profile

$$\Phi_{eq}(Z) = P_+ \Phi_{eq}^{+}(Z) + P_- \Phi_{eq}^{-}(Z), \qquad P_+ + P_- = 1 \tag{16}$$

satisfies Eq. (15). For large D both P_+ and P_- are close to $\frac{1}{2}$, and thus $\Phi_{eq}(Z) \approx 0$ apart from the narrow surface enrichment layers near the walls.

Note that one *does not obtain* this correct description of equilibrium, [Eqs. (15), (16)] if one simply solves the one-dimensional version of Eqs. (1)–(5), where the X-dependence is suppressed. Figure 2b, as a warning signal, gives an explicit demonstration that one gets a very different *metastable* solution from such a one-dimensional calculation. In fact, the character of this one-dimensional solution is nearly trivial to understand: the system must satisfy the boundary conditions, which require $\Phi_{eq}(Z = 0) \approx 1$, $\Phi_{eq}(Z = D) \approx 1$, together with the constraint that the total order parameter is zero [Eq. (15)]. The only way to do this in one dimension and find a minimum of the free energy functional is to place two interfaces between phases with the positive value of the order parameter (domains adjacent to the walls) and the negative value of the order parameter (in the center of the film). Any structure with more interfaces (such as the structures in Figs. 1a, 1b, 2a, and 2c) has a higher total inter-

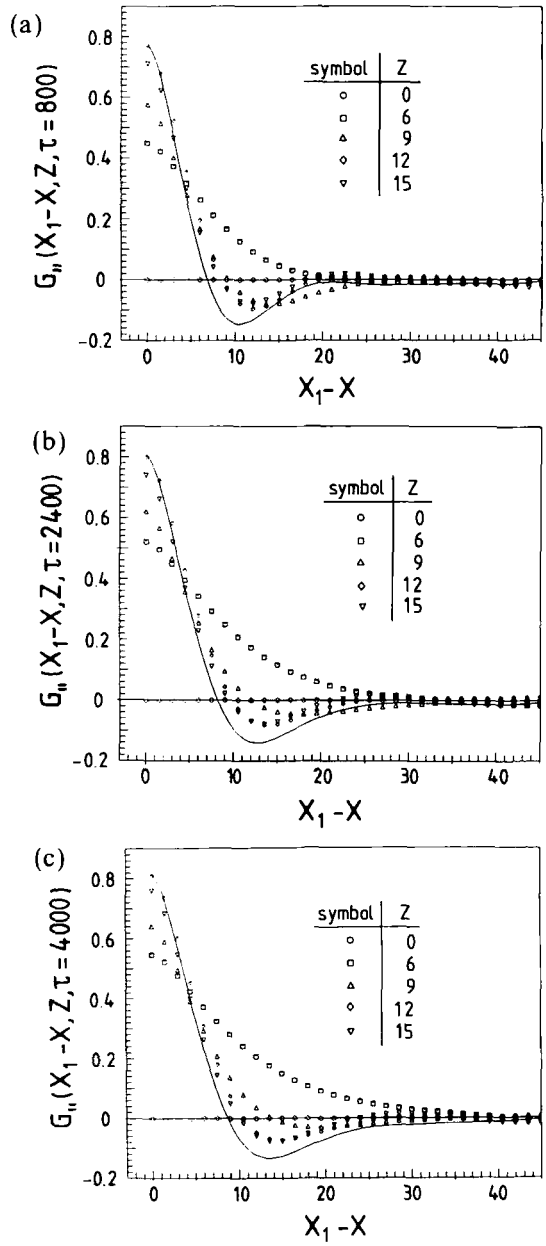

Fig. 3. Correlation functions in the direction parallel to the surface, $G_{\parallel}(X_1 - X, Z, \tau)$, plotted vs. distance $X_1 - X$ for different values of Z, as indicated in the figure, and three choices of τ: $\tau = 800$ (a), 2400 (b), and 4000 (c). Bulk behavior is shown for comparison (full curve). All data are for $D = 30$ and the same parameter values as in Fig. 1.

facial free energy than the state of Fig. 2b and hence can be at best metastable with respect to this state. Of course, the profile shown in Fig. 2b means that one has two interfaces running parallel to the walls throughout the total extension of the film. Thus the total interfacial energy of this configuration is $2L_x f_{\text{int}}$, where f_{int} is the (rescaled) interfacial tension of our model [which can be calculated from Eq. (8) by imposing boundary conditions $\Phi_s(\mathbf{R}, Z \to \infty) = +1$, $\Phi_s(\mathbf{R}, Z \to -\infty) = -1$,[1,3,49,53] and obviously is of order unity in our scaled units of length, etc.] In contrast, such an interfacial contribution for the inhomogeneous solution postulated in Eq. (16) appears only for the profile $\Phi_{\text{eq}}^{-}(Z)$, but not for $\Phi_{\text{eq}}^{+}(Z)$, and hence the total interfacial energy of the suggested configuration in Eq. (16) is only $2P_{-} L_x f_{\text{int}}$ if the domains are very large in the X direction, which is always expected in $d = 3$ dimensions. (In equilibrium, there would only be two domains, and respecting the periodic boundary condition in the X direction, one needs two interfaces, which give an additional interfacial free energy cost of $2Df_{\text{int}}$, which is negligible for $L_x \gg D$). In $d = 2$ dimensions, the situation is somewhat more subtle since a strip of finite width D is a quasi-one-dimensional system. Thus, strictly speaking, the two-dimensional strip has no phase transition, and there is a finite linear dimension of the domains in the X direction even for $L_x \to \infty$, namely[54] $l_{||}^{\text{eq}} \propto \exp(2f_{\text{int}} D)$.

Thus the contribution of the interfaces running perpendicular to the walls to the total free energy is negligible also for $d = 2$ if $D \gg 1$, which is the situation considered: for $D \approx 1$ there is a large distortion of the phase diagram in the capillary[39–41] and hence the quench is still in the one-phase region for very small D. However, this situation is not considered here. In any case, we wish to emphasize that one-dimensional solutions of Eq. (1), which are rather popular in the literature because the computing effort is so much less and they can be run up to the final "equilibrium," necessarily *never* yield a description of an inhomogeneous equilibrium resulting from the superposition of coexisting phases, and as a rule will yield metastable states of little physical significance only. Figure 2b is a demonstration of this statement.

We next turn to a discussion of the correlation function $G_{||}(X_1 - X, Z, \tau)$; cf. Eq. (9) (Figs. 3–6). Figure 3a–3c show $G_{||}(X_1 - X, Z, \tau)$ for $D = 30$ at different values of Z and times $\tau = 800$, 2400, and 4000. As for the semi-infinite system,[26] at the surface ($Z = 0$) the correlation function vanishes, because there is a uniform positive order parameter with no fluctuations. Also for $Z = 6$, a position in the second enriched layer (cf. Figs. 2a and 2c), the correlation function exhibits little structure, it is close to a monotonic decay to zero and develops at best a shallow minimum. Only deeper in the bulk does the correlation function develop the characteristic minimum, which is the hallmark of a spinodally decomposing system.[10–13] Corre-

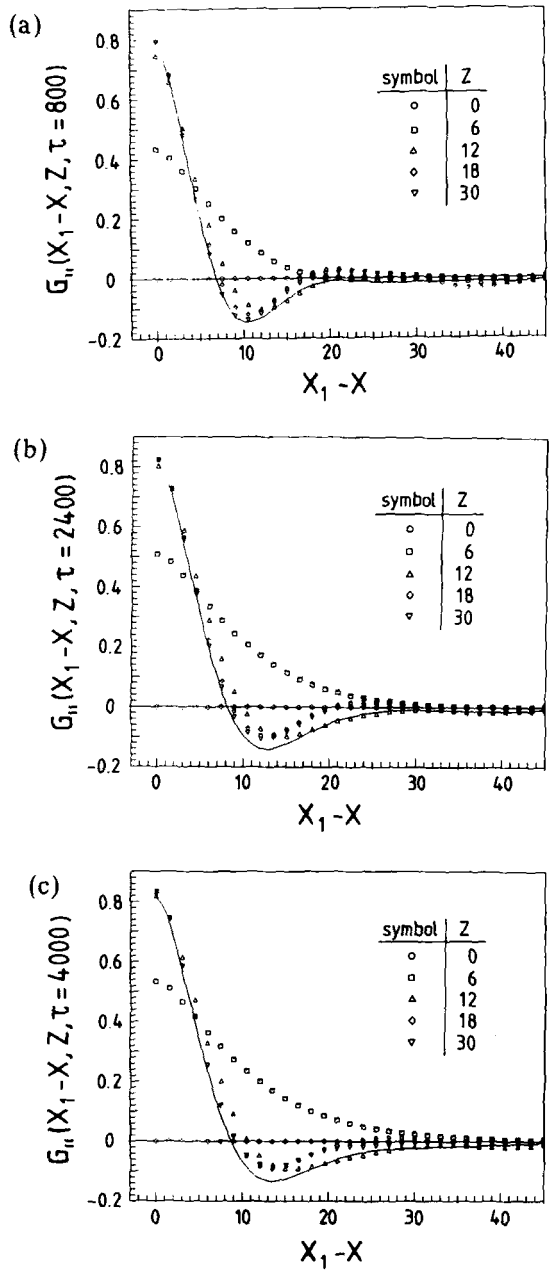

Fig. 4. Same as Fig. 3, but for $D = 60$.

sponding data for the correlation function for the film with $D = 60$ are shown in Fig. 4. While for the smaller thickness ($D = 30$) the correlation function in the center of the film deviates from its bulk counterpart (shown as a solid line) already at rather early times ($\tau = 800$, Fig. 3a), for the thicker film ($D = 60$) the data at early times for the correlation function in the center of the film agree with bulk behavior quantitatively (Fig. 4a), and

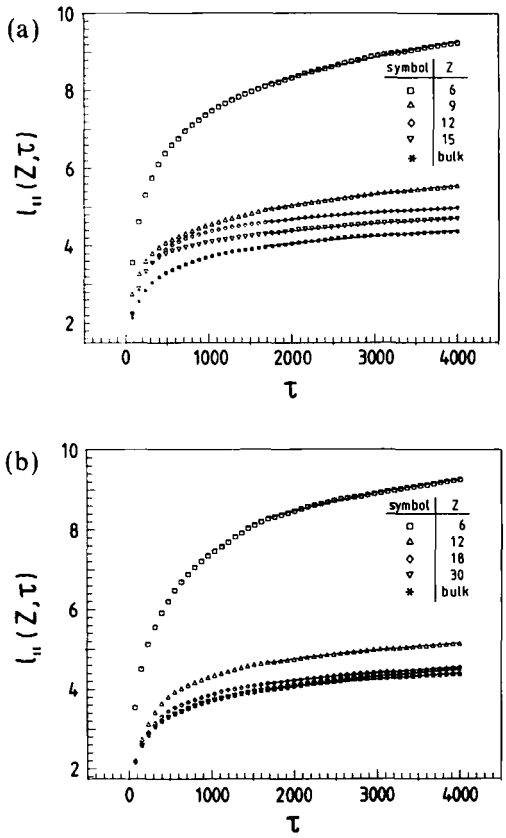

Fig. 5. Time dependence of the length scales in the direction parallel to the surfaces, $l_{||}(Z, \tau)$, for four values of Z, as indicaed in the figure, for $D = 30$ (a) and $D = 60$ (b). The bulk behavior is shown by asterisks. These lengths are defined as the distance at which the correlation functions $G_{||}(X_1 - X, Z, \tau)$ (Figs. 3 and 4) fall to half their initial values [Eq. (10)]. The data for $\tau > 1600$ are fitted to the power-law form $l_{||}(Z, \tau) = \alpha + \beta\tau^a$ (curves through the symbols) by the fitting procedure described in the text. The resulting "effective exponents" are, for $D = 30$, $a = 0.32$ ($Z = 6$), 0.30 ($Z = 9$), and 0.29 ($Z = 15$); and for $D = 60$, $a = 0.32$ ($Z = 6$), 0.30 ($Z = 12$), and 0.29 ($Z = 18$, $Z = 30$); the bulk exponent over this range of times is $a = 0.29$. The error bar on the growth exponents is ± 0.02.

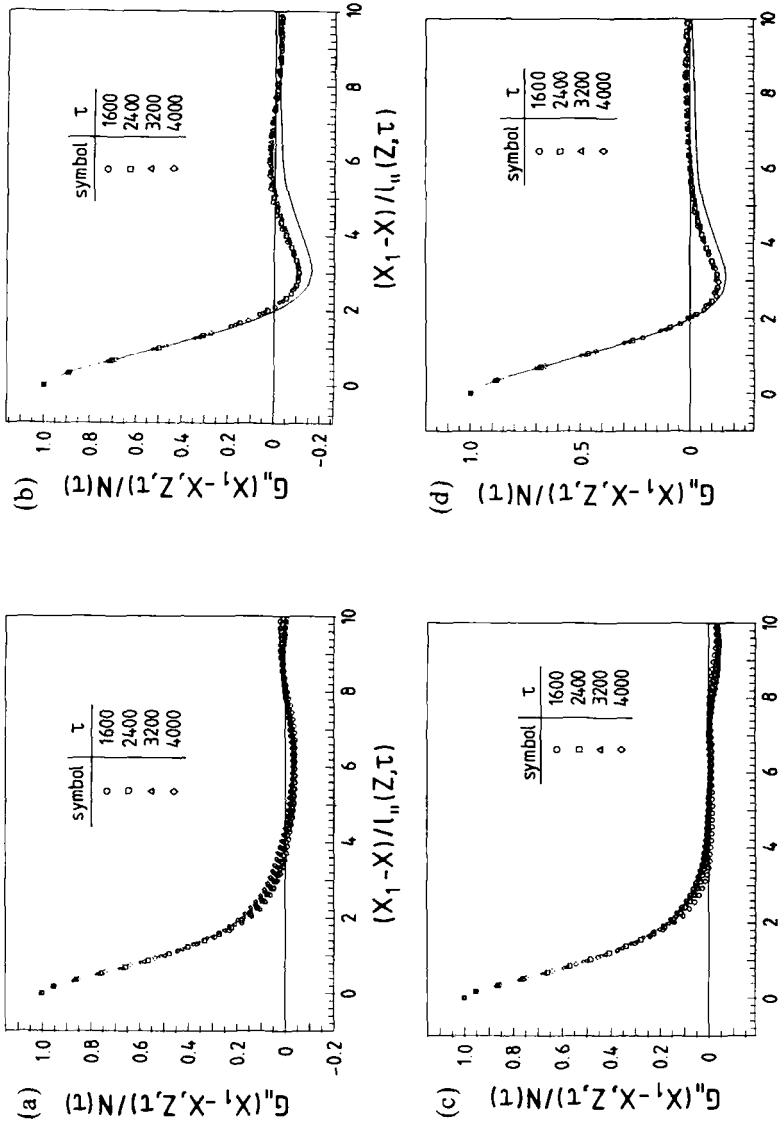

Fig. 6. Correlation functions $G_{\parallel}(X_1 - X, Z, \tau)$ normalized by their maximum values $N(\tau) \equiv G_{\parallel}(0, Z, \tau)$ plotted as a function of the scaled variable $(X_1 - X)/l_{\parallel}(Z, \tau)$ for times $\tau = 1600$, 2400, 3200, and 4000 (as indicated by different symbols) and the choices $D = 30$, $Z = 6$ (a), $D = 30$, $Z = 15$ (b), $D = 60$, $Z = 6$ (c), and $D = 60$, $Z = 30$ (d). Full curves in cases (b) and (d) show the corresponding scaling function of a bulk system.

only at later times when the characteristic linear dimension $l_{||}(Z, t)$ has grown rather large is the finite film thickness also felt by the time evolution of the growing domains in the center of the film, and $G_{||}(X_1 - X, Z = D/2, \tau)$ starts to deviate increasingly from the bulk behavior.

The time evolution of the characteristic linear dimension $l_{||}(Z, \tau)$ obtained from the correlation function [Eq. (10)] is shown in Fig. 5. One can see that $l_{||}(Z, \tau)$ is larger for small Z—this simply reflects the fact that the growing domains typically have a rather elongated shape and near the walls are oriented parallel to the walls, as is obvious from a glance at the snapshot pictures in Fig. 1—but otherwise the time evolution for all Z is rather similar. Since we expect that the characteristic linear dimension exhibits a power-law growth,[1-3,6-13,26,55] we have attempted to fit the data points for $\tau > 1600$ to a power law of the form $l_{||}(\tau) = \alpha + \beta\tau^{\alpha}$. Since this form contains three parameters, and the available time range is rather limited, a meaningful fit is nontrivial to carry out. We have found it useful to consider the auxiliary function[26]

$$f(Z, \tau) = [l_{||}(Z, \tau_2) - l_{||}(Z, \tau)]/[l_{||}(Z, \tau_2) - l_{||}(Z, \tau_1)] \tag{17}$$

where τ_1, τ_2 are the boundaries of the time interval we wish to fit ($\tau_1 = 1600$ and $\tau_2 = 4000$ in this case). This function eliminates the parameters α and β and leaves a single parameter (namely a) to be deermined. Using a nonlinear fitting routine, the data (100 points) can be well fitted (as shown by the curves in Fig. 5), and the effective exponents a are as indicated in the figure caption. As mentioned in the introduction, bulk spinodal decomposition gives an asymptotic exponent $a = \frac{1}{3}$ (Lifshitz–Slyozov growth[6,10-13,55]), but the approach to this asymptotic behavior is known to be rather slow,[10-13] and thus for the range of times studied here a somewhat smaller effective exponent is found, $a \approx 0.29$, consistent with previous experience.[10-13] The effective exponent close to the wall is somewhat enhanced, which is probably due to the fact that the data are affected by the existence of the enrichment and depletion layers near the wall, which are homogeneous in the X direction and slowly growing in thickness,[26] and therefore affecting the data for $l_{||}(Z, \tau)$ at small Z. Note also that the data for $Z = 6$ are practically identical for both values of D shown, and furthermore agree with corresponding results for the semiinfinite case. Also for $Z = 12$ the dependence on film thickness is rather small.

A long-standing idea on the dynamics of spinodal decomposition in the bulk has been the concept of dynamical scaling,[7] i.e., the correlation function depends on time only through the ratio of the considered distance to the characteristic length scale. This is tested in Fig. 6, where we superpose scaled correlation functions as a function of scaled lengths at different

times. It is seen that for $Z=6$, deviations from scaling are rather pronounced both for $D=30$ and $D=60$. For small values of Z, the data do not collapse well on a master curve, but rather deviate systematically (Figs. 6a and 6c). Of course, such deviations again reflect the influence of the slowly growing surface enrichment layer[26] and hence are not unexpected. In the center of the film a rather good scaling is observed (Figs. 6b and 6d), although the scaling functions do depend somewhat on film thickness and thus approach the bulk behavior (shown as a solid line) rather slowly.

In Fig. 7 we study the analogous scaling behavior of the integrated correlation function $G^{\text{int}}(X_1 - X, \tau)$ [defined in Eq. (11)]. It is seen that

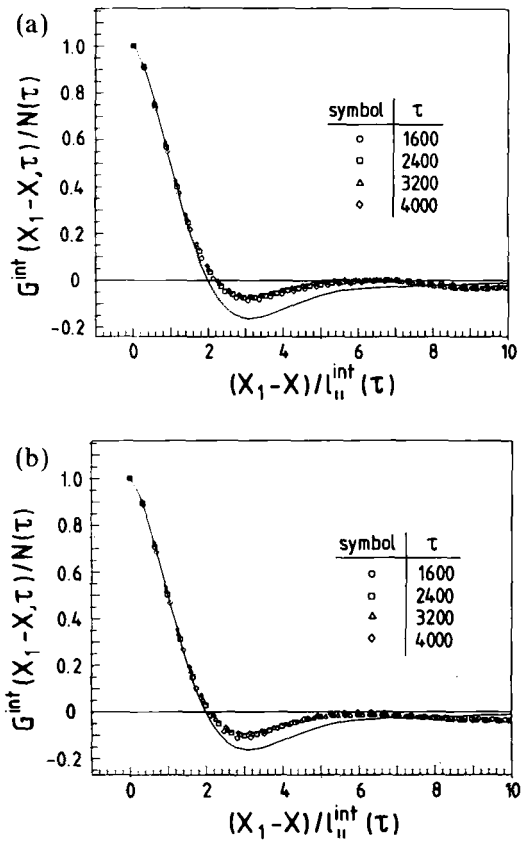

Fig. 7. Integrated correlation functions $G^{\text{int}}(X_1 - X, \tau)$ [Eq. (11)] normalized by their maximum values $N(\tau) \equiv G^{\text{int}}(0, \tau)$, plotted as a funcion of the scaled variable $(X_1 - X)/l_{\parallel}^{\text{int}}(\tau)$ for times $\tau = 1600$, 2400, 3200, and 4000 (as indicated by different symbols) for $D=30$ (a) and $D=60$ (b). Full curves show the corresponding scaling function of a bulk system.

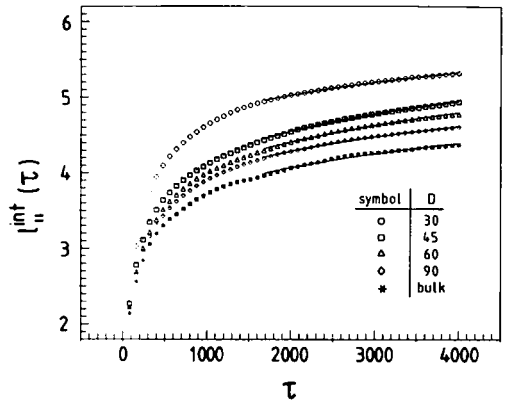

Fig. 8. Time dependence of the integrated length scale $l_{\parallel}^{\text{int}}(\tau)$ [cf. Eq. (12)] plotted vs. τ for four choices of the film thickness D as indicated in the figure. Asterisks show the bulk behavior. The data for $\tau > 1600$ are fitted to the power-law form $l_{\parallel}^{\text{int}}(\tau) = \alpha + \beta\tau^{a}$ (curves through the symbols) in exactly the same manner as done for $l_{\parallel}(Z, \tau)$. The resulting effective exponents are $a = 0.30$ ($D = 30$), $a = 0.29$ ($D = 45$), $a = 0.28$ ($D = 60$), and $a = 0.29$ ($D = 90$). The bulk exponent over this range of times as estimated from one-dimensional data is $a = 0.29$. The error bar on the growth exponent values is ± 0.02.

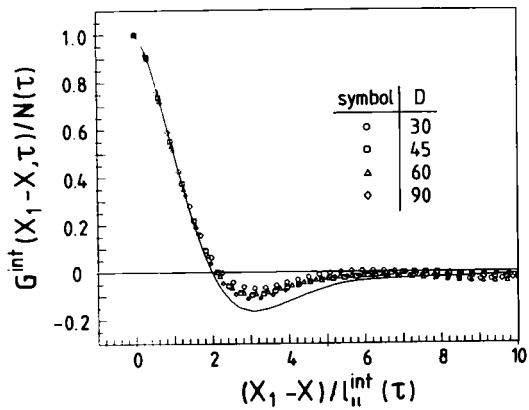

Fig. 9. Integrated correlation functions $G^{\text{int}}(X_1 - X, \tau)$ [Eq. (11)] normalized by their maximum values $N(\tau) \equiv G^{\text{int}}(0, \tau)$ plotted as a function of the scaled variable $(X_1 - X)/l_{\parallel}^{\text{int}}(\tau)$ for the dimensionless time $\tau = 3200$ and four different film thicknesses, as indicated by different symbols. Full curve shows the corresponding scaling function for the bulk system.

despite the disturbances that the walls create on the growing patterns (Figs. 1a and 1b) one observes a nearly perfect data collapse—only a close look reveals small but systematic deviations. The length scale $l_{||}^{\text{int}}(\tau)$ used to scale these data depends on film thickness D only slightly and its time dependence is rather similar to the bulk behavior for the time range studied (Fig. 8).

Figure 9 compares the scaling functions for $G^{\text{int}}(X_1 - X, \tau)$ for different thicknesses. Although the general shape of these functions is similar, the minimum is distinctly shallower than in the bulk, and the convergence

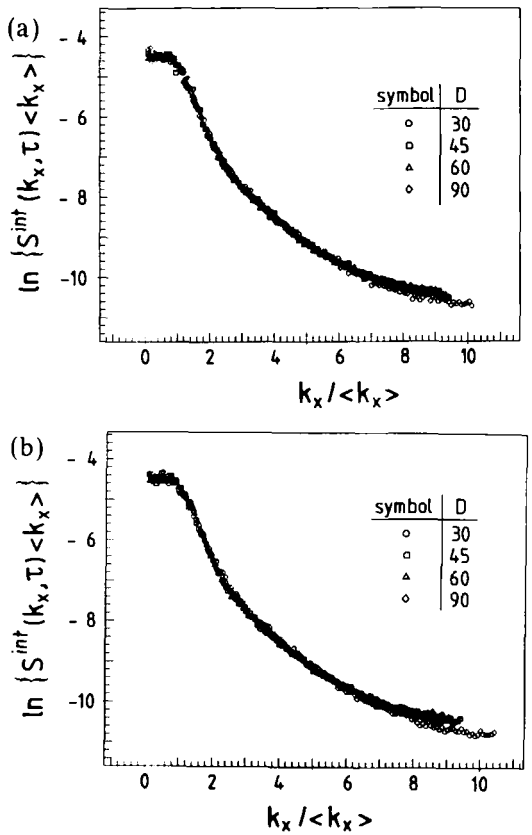

Fig. 10. Scaling plot of the normalized scattering function $S^{\text{int}}(k_x, \tau)\langle k_x\rangle$ versus the normalized momentum transfer $k_x/\langle k_x\rangle$ in a semilog plot. Here $\langle k_x\rangle = \int k_x S^{\text{int}}(k_x, \tau)\, dk_x$ is the first moment of the normalized scattering function and its inverse $\langle k_x\rangle^{-1}$ can also be considered as a measure of the characteristic length scale.[1-4,7-9] Four different film thicknesses are shown by different symbols. (a) $h_1 = 4$; (b) $h_1 = 8$. The surface field value $h_1 = 8$ corresponds to a wet static equilibrium in a semiinfinite geometry.

toward bulk behavior is rather slow in the regime of the minimum. Finally, we turn to the Fourier transform of $G^{\text{int}}(X_1 - X, \tau)$, the scattering function $G^{\text{int}}(k_x, \tau)$. Figure 10 shows the scaled scattering function as a function of the scaled wavevector for different values of film thickness D on a semilog plot. We have not included the point corresponding to $K_x = 0$, where $G^{\text{int}}(0, \tau) = 0$, by conservation of order parameter. This quantity is of particular interest, as it would be experimentally accessible. Since

Fig. 11. Snapshot pictures of the time evolution from one discrete implementation of the partial differential equation, as in Fig. 1, but for $h_1 = 8$, with $L_x = 600$ and $D = 30$ (a) and $D = 60$ (b). The snapshots refer to the scaled times (from left to right) $\tau = 50$, 100, 200, 500, 1000, and 4000.

$G^{\text{int}}(X_1 - X, \tau)$ showed approximately scaling behavior, it is no surprise that a similar scaling behavior must be found for its Fourier transform, $G^{\text{int}}(k_x, \tau)$. However, we add a caveat: the time range is rather short and is essentially the region dominated by two-dimensional growth. From Fig. 8 it is evident that the average linear dimensions $l_{\parallel}^{\text{int}}(\tau)$ are still much smaller than the linear dimension of the film. Since $l_{\parallel}^{\text{int}}(\tau)$ grows only rather slowly in the scaling regime $[l_{\parallel}^{\text{int}}(\tau) = \alpha + \beta\tau^a$ with $a \approx \frac{1}{3}]$, this behavior would not change even if we add another decade in simulation time. Only for substantially larger time scales, which are not accessible to our simulation for reasonably large film thicknesses, do we expect that $l_{\parallel}^{\text{int}}(\tau)$ becomes

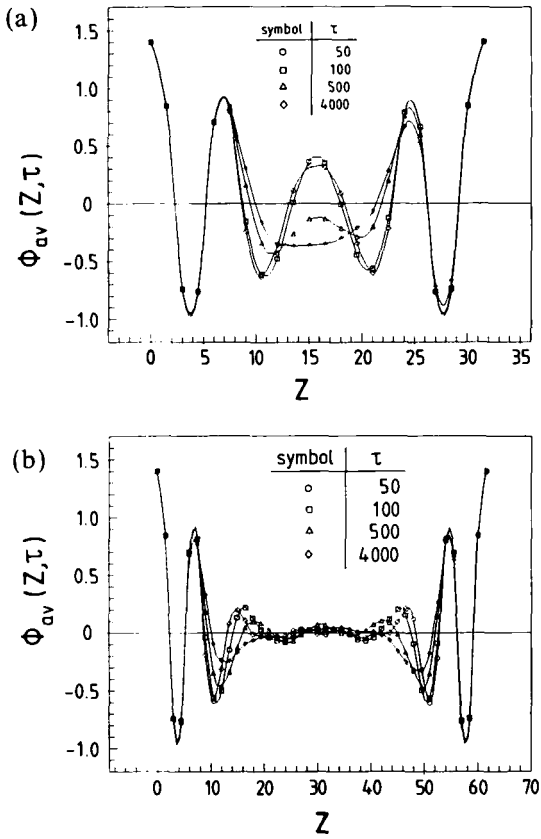

Fig. 12. Laterally averaged order profiles $\Phi_{\text{av}}(Z, \tau)$ plotted vs. the dimensionless distance Z from the first wall for four different scaled times as indicated, for $D = 30$ (a) and $D = 60$ (b). Parameters chosen are $\gamma = 4$, $g = -4$, and $h_1 = 8$, as in Fig. 11. Again the averages are obtained over 200 independent runs.

comparable to D and then a crossover to quasi-one-dimensional growth sets in, dominated by the diffusion of domain walls that are oriented perpendicular to the walls. In this crossover region, one may anticipate again clear deviations from the simple scaling as shown above. The scaling behavior studied in the present regime can be estimated to be valid over a time range of $10^3 \lesssim \tau \lesssim 10D^3$, and for $D = 60$ the upper limit of this range is indeed of the order of 10^6.

As the final results of this section, we discuss the dynamical behavior for boundary forces that would lead to a wet state of the surface in a semi-infinite geometry.[26] Both the comparison of the snapshot pictures (Figs. 1 and 11) and of the average profiles (Figs. 2 and 12) reveal that the behavior of the decomposing film is only little affected by this change in boundary condition. In our earlier study of surface effects on spinodal decomposition in semiinfinite geometry[26] we have shown that the growth of the thickness of the wetting layer, though present, is so much slower (namely logarithmic in time) than the Lifshitz–Slyozov growth of the phase-separated domains in the interior, and that this thickness hardly changes on the time scales of interest for spinodal decomposition. Thus the main distinction is that now the order parameter in the enrichment layers adjacent to the walls is enhanced to a value distinctly larger than unity (Fig. 12), which was not the case for the boundary condition corresponding to the incompletely wet state (Fig. 2).

As a consequence of the above considerations, the behavior of the correlation functions $G_{||}(X_1 - X, Z, \tau)$ and of the associated length scales $l_{||}(Z, \tau)$ turn out to be very similar to their counterparts in the case where the boundary field $h_1 = 4$ (the incompletely wet case) and for the sake of saving space we do not show these data here. As a representative example, we only present the scaling behavior of the integrated intensities (Fig. 13) and the associated time-dependent length scale $l_{||}^{\text{int}}(\tau)$ (Fig. 14). The scaled scattering function has already been anticipated in Fig. 10b and is also hardly distinguishable from its nonwet counterpart. Qualitatively the behavior is exactly as in the "nonwet" case, although for comparable thickness D and similar times τ the length scale $l_{||}^{\text{int}}(\tau)$ is slightly larger in this case. In this way, wetting of the surfaces leads to a small enhancement of the rate at which phase separation occurs in a thin film. But again the quantitative differences between Figs. 7, 9, and 11 are minor. In view of the various experimental claims on the strong effects of wetting layers on the kinetics of spinodal decomposition[18,19,22] this result is certainly somewhat unexpected! Of course, it should always be kept in mind that our modeling and results are for the case where the wall exerts a short-range force on the binary mixture and there are no hydrodynamic effects. Experimental systems need not necessarily conform to our simple picture.

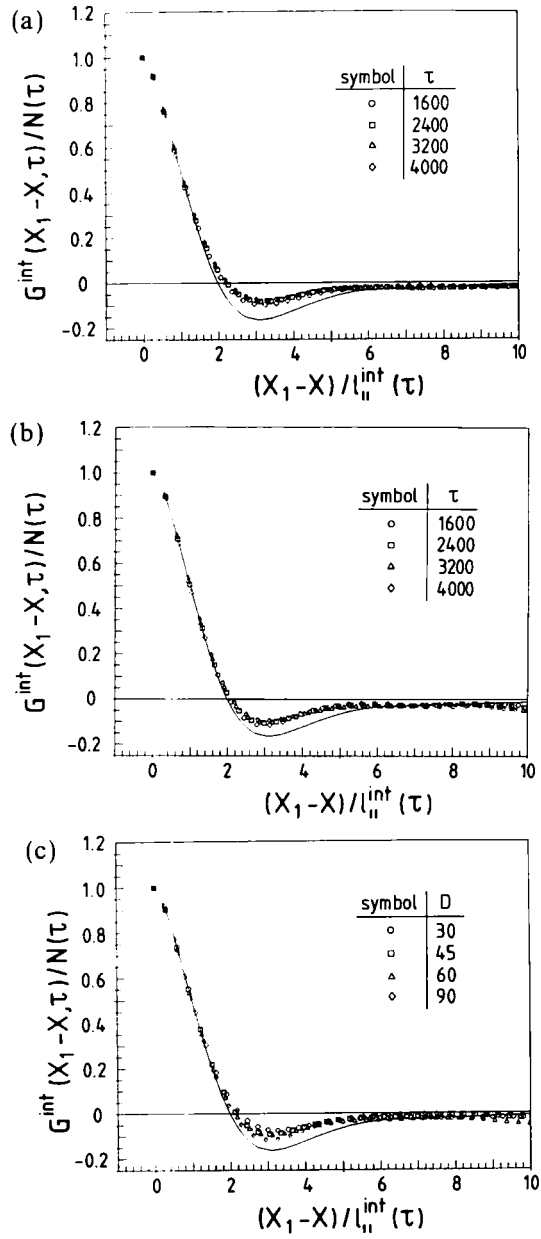

Fig. 13. Integrated correlation functions $G^{int}(X_1 - X, \tau)$ [Eq. (11)] normalized by their maximum values $N(\tau) \equiv G^{int}(0, \tau)$ plotted as a function of the scaled variable $(X_1 - X)/l_{||}^{int}(\tau)$ for the times $\tau = 1600$, 2400, 3200, and 4000 (as indicated by different symbols) for $D = 30$ (a) and $D = 60$ (b). Full curves show the corresponding scaling function of a bulk system. (c) An analogous scaling plot, but now $\tau = 3200$ is fixed and four film thicknesses are shown. Parameter values are as in Fig. 11.

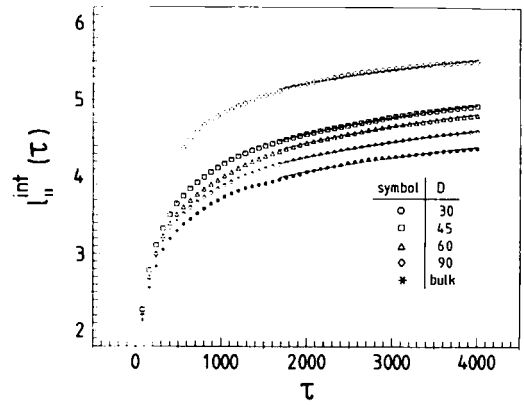

Fig. 14. Time dependence of the integrated length scale $l_{\parallel}^{\mathrm{int}}(\tau)$ [cf. Eq. (12)] plotted vs. τ for the four choices of the film thickness D indicated in the figure, as in Fig. 8, but for $h_1 = 8$ instead of $h_1 = 4$. The fits to the power law $l_{\parallel}^{\mathrm{int}}(\tau) = \alpha + \beta\tau^a$ are included and yield effective exponents which are only slightly larger for $D \leqslant 60$ than in Fig. 8: $a = 0.31$ ($D = 30$), 0.30 ($D = 45$), and 0.29 ($D = 60$, 90, and bulk). The error bar on the growth exponent is ± 0.02.

4. SUMMARY AND DISCUSSION

In this study, numerical calculations were presented to describe spinodal decomposition of binary mixtures in a thin-film geometry. We consider the case of two equivalent walls which energetically prefer one component and thus create an interplay between the formation of surface-enriched layers adjacent to the wall and spinodal decomposition. For simplicity, we have chosen a two-dimensional geometry (with one-dimensional walls), since our numerical method (which in the static equilibrium case would reduce to a Ginzburg–Landau-type treatment) makes little difference between $d = 2$ and $d = 3$ dimensions. We have argued, however, that one-dimensional versions of the theory would miss important physical effects, since then only interfaces parallel to the wall are possible, since no inhomogeneity in the X direction is allowed and interfaces perpendicular to the wall are suppressed. Arguments have been presented which suggest that for large D the equilibrium state toward which the system develops must contain such interfaces perpendicular to the walls.

We also emphasize that it is important to choose the correct boundary conditions, Eqs. (2)–(5), which have been motivated both from microscopic spin-exchange kinetic Ising models[14,20] and from general symmetry principles.[21] Since these boundary conditions are of the relaxational type for the local order parameter at the walls [Eqs. (2) and (4)], they lead to rapid establishment of local equilibrium at the walls, i.e., a thin surface-

enriched layer at the walls is formed, which necessitates the formation of an adjacent depletion layer, since the conservation law for the order parameter has to be respected. Inside this structure dominated by the walls, kinetics of spinodal decomposition proceeds more or less as usual, the only effect of the walls being that the orientation of elongated domains near the walls is predominantly parallel to the walls, i.e., the linear dimension $l_{||}(Z, \tau)$ near the walls is enhanced. In the average parallel linear dimension $l_{||}^{\text{int}}$ this phenomenon leads to a slight enhancement as D decreases, of course, since the surface region affects a relatively larger fraction of the film, the smaller is D. Apart from this trivial thickness effect, there is little dependence on D visible in the time range studied. However, for much larger times we expect that an interesting thickness dependence should occur, due to a crossover to quasi-one-dimensional growth when $l_{||}^{\text{int}}(\tau)$ is of the order of D and there should not be any inhomogeneity in the Z direction (apart from the thin surface enrichment layers at the walls).

For small D one expects that the unmixing transition temperature of the thin film is shifted to lower temperatures, and also the critical composition is shifted, since the boundary fields [Eqs. (6) and (7)] break the symmetry of the bulk model [Eq. (8)] with respect to a change of sign of the order parameter. It then is possible to consider quenches that stay outside the phase coexistence curve of the thin film, although they would be in the two-phase coexistence region of the bulk system. Such cases have not been considered here, however, because we feel an appropriate treatment of the inhomogeneous equilibrium profiles that then develop in the thin film requires a treatment beyond Ginzburg–Landau theory. While the cell-dynamics methods[11] used here are adequate for the late stages of spinodal decomposition (thermal fluctuation effects can then be neglected, as the fluctuations contained in the initial state are deterministically amplified), this technique is not suitable to describe critical phenomena such as associated with the shape of a two-phase coexistence region and its change in a thin-film geometry, etc.

An obvious and interesting extension of the present treatment would be the consideration of off–critical quenches and/or asymmetric boundary fields. Note also that we have considered just two typical cases of parameters in the boundary conditions, but a more systematic scan of what these boundary terms can effect should also be worthwhile. The present paper can be considered as a modest first step only, although the physical situation is much simpler and clear-cut than in the experiments. Nevertheless we hope that the present work will contribute to a better interpretation of these experiments as well.

ACKNOWLEDGMENTS

S. P. expresses his gratitude to the Deutsche Forschungsgemeinschaft (DFG) for partial support under Sonderforschungsbereich 262. The authors acknowledge stimulating discussions with H. L. Frisch and J. Klein.

REFERENCES

1. J. D. Gunton, M. San Miguel, and P. S. Salmi, In *Phase Transitions and Critical Phenomena*, Vol. 8, C. Domb and J. L. Lebowitz, eds. (Academic Press, London, 1983), p. 267.
2. S. Komura and H. Furukawa, eds., *Dynamics of Ordering Processes in Condensed Matter* (Plenum Press, New York 1988).
3. K. Binder, In *Materials Science and Technology, Vol. 5: Transformations in Materials*, R. W. Cahn, P. Haasen, and E. J. Kramer, eds. (VCH, Weinheim, 1991), p. 405.
4. G. Kostorz, preprint.
5. J. W. Cahn and J. E. Hilliard, *J. Chem. Phys.* **28**:258 (1958); J. W. Cahn, *Acta Metall.* **9**:795 (1961).
6. I. M. Lifshitz and V. V. Slyozov, *J. Phys. Chem. Solids* **19**:35 (1961).
7. K. Binder and D. Stauffer, *Phys. Rev. Lett.* **33**:1006 (1974); *Z. Phys. B* **24**:406 (1976).
8. A. B. Bortz, M. H. Kalos, J. L. Lebowitz, and M. A. Zendejas, *Phys. Rev. B* **10**:535 (1974).
9. J. Marro, A. B. Bortz, M. H. Kalos, and J. L. Lebowitz, *Phys. Rev. B* **12**:2000 (1975); M. H. Kalos, J. L. Lebowitz, O. Penrose, and A. Sur, *J. Stat. Phys.* **18**:39 (1978).
10. D. Huse, *Phys. Rev. B* **34**:7845 (1986).
11. Y. Oono and S. Puri, *Phys. Rev. Lett.* **58**:836 (1987); Y. Oono and S. Puri, *Phys. Rev. A* **38**:434 (1988); S. Puri and Y. Oono, *Phys. Rev. A* **38**:1542 (1988); A. Shinozaki and Y. Oono, *Phys. Rev. Lett.* **66**:173 (1991).
12. T. M. Rogers, K. K. Elder, and R. C. Desai, *Phys. Rev. B* **37**:196 (1988); A. Chakrabarti and J. D. Gunton, *Phys. Rev. B* **37**:3798 (1988).
13. J. G. Amar, F. E. Sullivan, and R. D. Mountain, *Phys. Rev. B* **37**:196 (1988).
14. K. Binder and H. L. Frisch, *Z. Phys. B* **84**:403 (1991).
15. R. A. L. Jones, L. J. Norton, E. J. Kramer, F. S. Bates, and P. Wiltzius, *Phys. Rev. Lett.* **66**:1326 (1991).
16. P. Wiltzius and A. Cumming, *Phys. Rev. Lett.* **66**:3000 (1991).
17. U. Steiner, E. Eiser, J. Klein, A. Budkowski, and L. J. Fetters, *Science* **258**:1126 (1992).
18. F. Bruder and R. Brenn, *Phys. Rev. Lett.* **69**:624 (1992).
19. H. Tanaka, *Phys. Rev. Lett.* **70**:53 (1992).
20. S. Puri and K. Binder, *Phys. Rev. A* **46**:R4487 (1992); S. Puri and H. L. Frisch, *J. Chem. Phys.*, in press.
21. H. W. Diehl and H.-K. Janssen, *Phys. Rev. A* **45**:7145 (1992).
22. B. Q. Shi, C. Harrison, and A. Cumming, *Phys. Rev. Lett.* **70**:206 (1993).
23. J. F. Marko, *Phys. Rev. E* **48**:2861 (1993).
24. G. Krausch, C.-A. Dai, E. J. Kramer, J. F. Marko, and F. S. Bates, *Macromolecules* **26**:5566 (1993); G. Krausch, E. J. Kramer, F. S. Bates, J. F. Marko, G. Brown, and A. Chakrabarti, preprint.
25. G. Brown and A. Chakrabarti, *Phys. Rev. A* **46**:4829 (1992).
26. S. Puri and K. Binder, *Phys. Rev. E* **49**:5359 (1994).

27. S. Dietrich, In *Phase Transitions and Critical Phenomena*, Vol. 12, C. Domb and J. L. Lebowitz, eds. (Academic Press, New York, 1988), p. 1.
28. D. E. Sullivan and M. M. Telo da Gama, in *Fluid Interfacial Phenomena*, C. A. Croxton, ed. (Wiley, New York, 1986), p. 45.
29. P. G. de Gennes, *Rev. Mod. Phys.* **57**:827 (1985).
30. M. E. Fisher, *J. Stat. Phys.* **34**:667 (1984); *J. Chem. Soc. Faraday Trans.* **282**:1569 (1986).
31. R. Lipowsky and D. A. Huse, *Phys. Rev. Lett.* **52**:353 (1986).
32. M. N. Barber, In *Phase Transitions and Critical Phenomena*, Vol. 8, C. Domb and J. L. Lebowitz, eds. (Academic Press, New York, 1983), p. 156.
33. K. Binder, *Ferroelectrics* **73**:43 (1987).
34. V. Privman, ed., *Finite Size Scaling and the Numerical Simulution of Statistical Systems* (World Scientific, Singapore, 1990).
35. K. Binder, *Annu. Rev. Phys. Chem.* **43**:33 (1992).
36. P. G. de Gennes, *Macromolecules* **13**:1069 (1980).
37. J.-S. Wang and K. Binder, *Macromol. Chem. Theory Simul.* **1**:49 (1992).
38. M. E. Fisher and Nakanishi, *J. Chem. Phys.* **75**:5857 (1981); H. Nakanishi and M. E. Fisher, *J. Chem. Phys.* **78**:3279 (1983).
39. D. Henderson, ed., *Fundamentals of Inhomogeneous Fluids* (M. Dekker, New York, 1992).
40. K. Binder and D. P. Landau, *J. Chem. Phys.* **96**:1444 (1992).
41. E. Siggia, *Phys. Rev. A* **20**:595 (1979).
42. H. Furukawa, *Physica A* **123**:497 (1984); *Adv. Phys.* **34**:703 (1985).
43. T. Koga and K. Kawasaki, *Phys. Rev. A* **44**:R817 (1991).
44. S. Puri and B. Dünweg, *Phys. Rev. A* **455**:R6977 (1992), A Shinozaki and Y. Oono, *Phys. Rev. E*, in press.
45. K. Kawasaki, In *Phase Transitions and Critical Phenomena*, Vol. 2, C. Domb and M. S. Green, eds. (Academic Press, London, 1972), Chapter 11.
46. K. Binder, *Z. Phys.* **267**:313 (1974).
47. R. C. Ball and R. L. H. Essery, *J. Phys.: Condensed Matter* **2**:10303 (1990).
48. J. Rowlinson and B. Widom, *Molecular Theory of Capillarity* (Oxford University Press, Oxford, 1982).
49. I. Schmidt and K. Binder, *Z. Phys. B* **67**:369 (1987).
50. S. Puri and K. Binder, *Z. Phys. B* **86**:263 (1992).
51. D. Nicolaides and R. Evans, *Phys. Rev. B* **39**:9336 (1989).
52. B. Widom, In *Phase Transitions and Critical Phenomena*, Vol. 2, C. Domb and M. S. Green, eds. (Academic Press, London, 1972).
53. M. E. Fisher, *J. Phys. Soc. Japan Suppl.* **26**:87 (1969); see also G. G. Gabrera, R. Jullien, E. Brezin, and J. Zinn-Justin, *J. Phys.* (Paris) **47**:1305 (1986).
54. E. V. Albano, K. Binder, W. Paul, and D. W. Heermann, *Physica A* **183**:130 (1992); M. Müller and W. Paul, *J. Stat. Phys.* **73**:209 (1993).
55. K. Kawasaki and T. Ohta, *Physica A* **118**:175 (1983); T. Koga and K. Kawasaki, *Physica A* **196**:389 (1993); M. Tokuyama and Y. Enomoto, *Phys. Rev. E* **47**:1156 (1993).